Available online at www.sciencedirect.com
ScienceDirect
Journal of the European Ceramic Society 28 (2008) 353–365
www.elsevier.com/locate/jeurceramsoc

Effect of transition-metal-ion doping on high temperature thermal expansion of 3:2 mullite—An in situ, high temperature, synchrotron diffraction study

P. Sarin, W. Yoon, R.P. Haggerty, C. Chiritescu, N.C. Bhorkar, W.M. Kriven *

Department of Materials Science and Engineering, University of Illinois at Urbana-Champaign, IL 61801, USA

Available online 17 May 2007

Abstract

The effect of Ti^{4+}, Cr^{3+} or Ga^{3+} doping on thermal expansion of 3:2 mullite was examined from 20 °C to 1400 °C by high temperature XRD using synchrotron radiation. The room temperature mullite lattice expanded with metal-ion incorporation and the change in the *b*-axis was larger than that along the *a*-axis ($\Delta b > \Delta a$) for all ion types. Upon heating, the largest elongation was along the *b*-axis ($\Delta b/b_{RT}$) and was similar to that in the pure mullite (~0.5%). Least expansion was observed along the *a*-axis ($0.28\% \leq \Delta a/a_{RT} \leq 0.41\%$). The thermal expansion of mullite was not constant in the temperature range from 20 °C to 1400 °C, and had a linear dependence on temperature ($\alpha(T) = A_0 + A_1 \Delta T$). The α_{mean} values increased with temperature ($20\,^{\circ}C \leq T \leq 1000\,^{\circ}C$), but were always within 3.0–6.7. Cr^{3+} and Ga^{3+} doping decreased the anisotropy in mullite lattice expansion, however, Ti^{4+} doping showed a sharp increase. Trends associated with type and the quantity of dopant are discussed.

Keywords: Thermal expansion; Mullite; Transition metal-ion dopants

1. Introduction

Mullite is an important material in ceramic science and technology. Research on this material system, which spans well over a century including several studies being reported in recent years, highlight the significance of this material for both conventional and advanced ceramic applications.[1,2] Mullite is a strong candidate for advanced structural applications at high temperatures, because it has a high melting point, good creep resistance, superior high temperature strength, low thermal expansion, outstanding thermal shock resistance and displays exceptional chemical stability under harsh chemical environments. Amongst the several potential applications envisaged for mullite and mullite composites are thermal and environmental barrier coatings for aircraft and gas turbine engines, efficient catalytic converters, kiln furniture, hot gas filters, etc.

Mullite, described as substituted alumina by Cameron,[3] belongs to the family of aluminosilicates which can be represented by the general formula ($Al_2[Al_{2+2x}Si_{2-2x}]O_{10-x}$), where x ($0.18 \leq x \leq 0.88$) denotes the number of missing oxygen atoms per average unit cell.[4] The 3:2 mullite (for $x = 0.25$), i.e. $Al_2[Al_{2.5}Si_{1.5}]O_{9.75}$, is considered to be the most stable phase amongst others (2:1 mullite for $x = 0.40$; 3:1 mullite for $x = 0.57$). The structure of mullite consists of chains of edge-sharing AlO_6 octahedra oriented parallel to the crystallographic *c*-axis. These chains of octahedra are separated by (Si, Al)O_4 tetrahedra in an alternating sequence, forming double chains parallel to the *c*-axis.[2,5–9]

The 3:2 mullite has a highly stable open structure ($T_{Melt} = 1828 \pm 10\,^{\circ}C$)[10,11] and it can accommodate a variety of transition metal ions into its structure as a solid solution.[2] Such solid solutions can result in desirable improvements in physical properties such as thermal expansion behavior, electrical resistivity, etc. For example, incorporation of Mn^{2+}, Fe^{3+}, Cr^{3+}, or Ti^{4+} ions was shown to decrease electrical resistivity by two orders of magnitude at room temperature.[12] Similarly, thermal expansion behavior was altered by incorporation of Cr^{3+} and Fe^{3+} cations.[13,14] Several studies have been reported on the incorporation of metal-ion dopants in mullite.[12,15–27] From these studies it has been concluded that the mullite structure can incorporate differing amounts of ions, and that the limit of

* Corresponding author at: Department of Materials Science and Engineering, University of Illinois at Urbana-Champaign, 1304 West Green Street, Urbana, IL 61801, USA. Tel.: +1 217 333 5258; fax: +1 217 333 2736.
E-mail address: kriven@uiuc.edu (W.M. Kriven).

0955-2219/$ – see front matter © 2007 Elsevier Ltd. All rights reserved.
doi:10.1016/j.jeurceramsoc.2007.03.002

Table 1
Thermal expansion coefficients reported in literature for various types of metal-ion doped 3:2 mullite samples

	Wt.% dopant oxide	Thermal expansion coefficients ($\times 10^{-6}$)				Temperature range (°C)
		α_a	α_b	α_c	Mean α[a]	
Mullite	0	4.1	6.0	5.7	5.3	300–1000[13]
		3.9	7.0	5.8	5.6	300–900[14]
		6.8	9.3	6.3	7.5	1000–1600[13]
		5.4	7.1	6.5	6.3	800–1300[2]
		5.3	10.4	5.9	7.2	1300–1600[2]
Cr–mullite	11.5	3.6	5.9	5.2	4.9	300–1000[13]
		3.1	6.2	5.6	5.0	300–900[14]
		5.8	11.0	6.1	7.6	1000–1600[13]

[a] Mean $\alpha = (\alpha_a + \alpha_b + \alpha_c)/3$.

dopant ion incorporation depends on synthesis conditions, ionic radii and the oxidation states of transition metal ions.[2,28] While the highest degrees of incorporation were observed for trivalent cations such as V^{3+}, Cr^{3+} and Fe^{3+} (approximately 11–13 wt.% as oxides) followed by Ti^{4+}, and V^{4+} (2–6 wt.% as oxides), only very low amounts of Mn^{2+}, Fe^{2+} and Co^{2+} ions (<1 wt.% as oxides) entered the mullite structure.[2,15,19,20,23,28,29]

Mullites display low and non-linear thermal expansion below ~300 °C; and larger linear expansion between 300 °C and 1000 °C. Beyond 1000 °C, up to 1300 °C, an observed discontinuity in thermal expansion behavior has been attributed to a phase transformation, but is not completely understood.[2,30] Schneider and Eberhard,[14] and later Brunauer et al.[13] showed that incorporation of Cr^{3+} and Fe^{3+} (11.5 wt.% and 10.3 wt.%, respectively) in mullite resulted in a decrease in thermal volume expansion. Table 1 summarizes the thermal expansion coefficients of mullite and metal-ion doped mullites known so far.

The objective of this study was to systematically investigate the effect of transition metal-ion dopants on thermal expansion properties of mullite, up to 1400 °C in air. Three metal-ion dopants were evaluated in this study, and they included Ti^{4+}, Cr^{3+}, and Ga^{3+}. Variation of thermal expansion behavior was studied as a function of both the type and the concentration of transition metal-ion dopant incorporated into the mullite structure. All measurements were conducted on powder samples (synthesized using co-precipitation methods), and studied by high temperature X-ray diffraction (HTXRD) using synchrotron radiation. Temperature dependent thermal expansion coefficients were determined for each crystallographic axis of the orthorhombic mullite structure based on careful statistical analysis.

2. Materials and methods

The selection of candidate transition metal ions for incorporation in the mullite structure was made after thorough screening of the existing literature. Primary criterion for the choice of a transition metal-ion dopant was the similarity in ionic size in an octahedral field of O^{2-} anions. The ions were selected such that the effect of oxidation state and electronic configuration could also be evaluated. Based on the above guidelines, Ti^{4+}, Cr^{3+}, and Ga^{3+} were identified (see Table 2) as suitable candidates for this study.

2.1. Synthesis of metal-ion doped mullite powders

Powder samples of transition metal-ion doped mullite systems were synthesized by co-precipitation methods as shown in Fig. 1. While Ti-doped mullite samples were synthesized by the sol–gel method, Cr- and Ga-doped mullite samples were synthesized by the organic steric entrapment method using polyvinyl alcohol (PVA) as the steric agent. Both of these syntheses routes allow for mixing of cations at a molecular level and were therefore preferred over reaction sintering methods. Samples were synthesized to cover a large range of dopant ion concentration, up to the solubility limits of the respective metal-ions in the mullite structure, as reported in the literature. Moreover, the composition of the doped 3:2 mullite samples was proportionally altered taking into consideration the crystallographic location occupied by the metal ion in the mullite structure.[28] All the selected metal ions are believed to substitute for Al^{3+} in the AlO_6 octahedra, although, Cr^{3+} can also occupy interstitial sites.[23] In addition, the incorporation of Ti^{4+} at the Al^{3+} site in the oxygen octahedra further necessitates substitution of tetrahedral Si^{4+} by Al^{3+} for charge compensation.[28] Therefore, in the case of Cr- and Ga-doped mullite samples, the amount of Al^{3+} was proportionally reduced. However, in the case of Ti-doped mullites, the amount of Si^{4+} was proportion-

Table 2
Ionic radii,[44,45] valence state and electronic configuration of (a) cations present in the 3: 2 mullite, and (b) transition metal ions identified for this study

Element	Valence	Electron configuration	Ionic radii (pm)	
			Tetrahedral sites	Octahedral sites
Al	3+	$2p^6$	39.00	53.50
Si	4+	$2p^6$	26.00	40.00
Ti	4+	$3p^6$	42.00	60.50
Cr	3+	$3d^3$	–	61.50
Ga	3+	$3d^{10}$	47.00	62.00

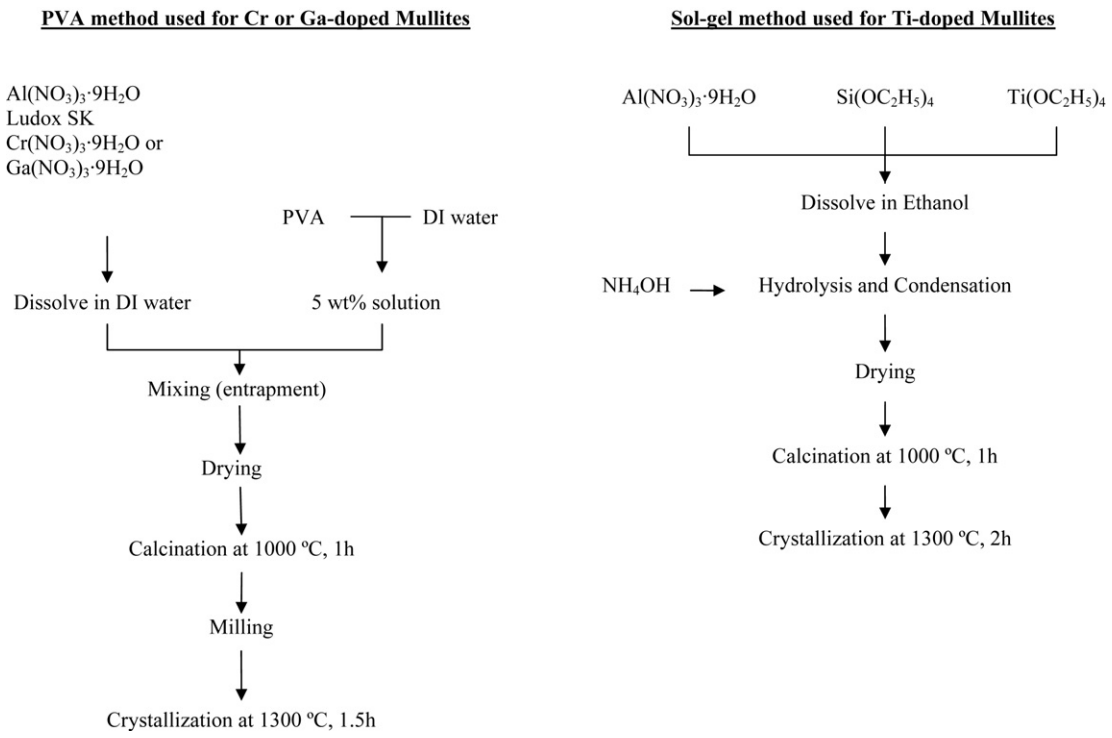

Fig. 1. Flow chart for synthesis of the metal-ion doped 3:2 mullite sample powders.

ally reduced in order to retain the overall 3:2 mullite composition.

Ti-doped mullite sols were prepared using aluminum nitrate ($Al(NO_3)_3{\cdot}9H_2O$), tetraethyl orthosilicate ($Si[OC_2H_5]_4$, or TEOS), and titanium ethoxide ($Ti[OC_2H_5]_4$). All chemicals were from Aldrich Chemical Company, Milwaukee, WI. The chemicals were first dissolved in ethanol in the desired proportions, and this was followed by hydrolysis and a condensation reaction by slow addition of ammonium hydroxide (NH_4OH) solution. The solution was constantly stirred up to gelation. The resultant gel was dried in an oven at 70 °C for 48 h before calcination at 1000 °C for 1 h. The calcined powder was further heat treated at 1300 °C for 2 h for complete crystallization. In addition to Ti-doped mullite samples, pure 3:2 mullite was also synthesized using the sol–gel method.

Cr- and Ga-doped mullite powders were prepared by the organic steric entrapment method using PVA as the steric agent.[11,31–36] A 5 wt.% PVA solution was prepared by dissolving partially hydrolyzed PVA powder (Celvol 205S, Celanese Corporation, Pasadena, TX) in deionized water, stirring continuously for over 24 h. $Al(NO_3)_3{\cdot}9H_2O$ and Ludox SK (25 wt.% SiO_2 colloidal solution, Dupont Chemicals) were used as sources of aluminum and silicon, respectively. Chromium nitrate nonahydrate ($Cr(NO_3)_3{\cdot}9H_2O$) and gallium nitrate nonahydrate ($Ga(NO_3)_3{\cdot}9H_2O$), both from Aldrich Chemical Company (Milwaukee, WI), were used as starting chemicals for the chromium and gallium additions, respectively. Three different compositions of Cr-doped mullites and five compositions of Ga-doped mullites were synthesized (see Table 3). The nitrate salts were dissolved in deionized water, followed by addition of Ludox solution. PVA solution was then added to the clear solution and stirring was continued for a further 1 h. The solution was then heated to evaporate water, and the resultant resin was then dried overnight at 110 °C. The dried mass was crushed using a mortar and pestle, calcined and crystallized at 1000 °C for 1 h and at 1300 °C for 2 h, respectively. The powder obtained was then attrition milled for 1 h, followed by further heat treatment at 1500 °C to ensure complete incorporation of the dopant ion into the mullite structure.

The chemical composition of sample powders was confirmed by energy dispersive spectroscopy (EDS) using the JEOL JSM-6060LV scanning electron microscope (SEM) (JEOL USA Inc., Peabody, MA, USA). The results are presented in Table 3. The crystalline content of the sample powders was verified by X-ray diffraction (Rigaku D-MaxII X-ray diffractometer, Rigaku, Danvers, USA).

2.2. *In situ high temperature synchrotron diffraction experiment*

High temperature X-ray diffraction is a powerful technique for measurement of physical properties such as thermal expansions and phase transformations, of ceramic materials. Using this technique, it is possible to determine the crystal structure of the material as a function of temperature, and thus study structural mechanisms that dominate both normal and anomalous expansion behavior. This method permits evaluation of thermal expansion of polycrystalline materials using crystallographic information and is not limited by microstructural flaws

Table 3
Composition of samples measured using SEM/EDS

Metal-ion	Sample ID	x	y	Al	Si	Mol% dopant cation	Al/Si	Oxide ratio in wt.% (Al_2O_3:SiO_2)
Mullite	M-0	0.00	0.00	5.65	2.00	0.00	2.83	70.6:29.4

Metal-ion	Sample ID	x	y	Al	Si	Mol% dopant cation	Al/(Si + M)	Oxide ratio in wt.% (Al_2O_3:SiO_2:TiO_2)
Ti	Ti-1	0.00	0.15	5.72	1.85	1.93	2.86	70.4:26.8:2.9
	Ti-2	0.00	0.24	5.50	1.76	3.13	2.75	69.2:26.1:4.6
	Ti-3	0.00	0.34	5.61	1.66	4.53	2.81	69.3:24.0:6.7

Metal-ion	Sample ID	x	y	Al	Si	Mol% dopant cation	(Al + M)/Si	Oxide ratio in wt.% (Al_2O_3:SiO_2:Cr_2O_3)
Cr	Cr-1	0.17	0.00	5.40	2.00	2.30	2.78	67.4:29.4:3.2
	Cr-2	0.55	0.00	5.35	2.00	6.96	2.95	62.8:27.6:9.6
	Cr-3	0.94	0.00	5.08	2.00	11.76	3.01	57.5:26.6:15.9

Metal-ion	Sample ID	x	y	Al	Si	Mol% dopant cation	(Al + M)/Si	Oxide ratio in wt.% (Al_2O_3:SiO_2:Ga_2O_3)
Ga	Ga-1	0.11	0.00	6.18	2.00	1.29	3.14	70.8:27.7:2.2
	Ga-2	0.26	0.00	5.45	2.00	3.35	2.85	65.9:28.4:5.7
	Ga-3	0.34	0.00	5.08	2.00	4.62	2.71	63.0:29.2:7.8
	Ga-4	0.46	0.00	5.37	2.00	5.82	2.91	62.7:27.5:9.8
	Ga-5	0.78	0.00	5.98	2.00	8.90	3.38	61.2:24.1:14.7

The general formula for 3:2 mullite is $Al_{6-x}M_{x+y}Si_{2-y}O_{13}$, where M = Ti, Cr, or Ga. Mol% dopant cation = [(moles of dopant cation)/(total number of moles of cations)] × 100.

such as porosity or presence of a secondary phase, which can compromise measurements made using other methods such as dilatometry.

In this study, the thermal expansion behavior of mullite and metal-ion doped mullite powder samples were evaluated using in situ high resolution X-ray diffraction (XRD) up to 1400 °C, in air. All measurements were conducted at the UNICAT beam line (33BMC) at the Advanced Photon Source (APS) at Argonne National Laboratory, Argonne, IL.

In a typical HTXRD experiment, powder specimens were heated, and the crystal structural changes were simultaneously recorded as XRD patterns. Powder specimens were mounted in 0.3 mm diameter fused quartz capillary (Charles Supper Company, Natick, MA, USA) and heated using a quadrupole lamp furnace (QLF).[37,38] The QLF is a radiation heating furnace, and can be used to conduct HTXRD investigations of ceramics in air up to 2000 °C in air.[37,38] XRD patterns were acquired at high temperatures over the range of 2–35° in 2θ, using the newly designed one-dimensional curved image plate (CIP) detector. The details of the construction, operation and capabilities of the CIP detector are reported elsewhere.[39,40] The CIP detector was aligned and calibrated using a Si(1 1 1) analyzer crystal and the LaB_6 powder standard for XRD (SRM 660a, National Institute of Standards and Technology, Gaithersburg, MD). Incident monochromatic X-rays of two different wavelengths, 0.550784 Å and 0.563084 Å, as calibrated with SRM 660a, were used in this work.

X-ray diffraction patterns were acquired in transmission geometry in steps of ∼100 °C, from room temperature up to ∼1400 °C. Fine Pt powder (0.15–0.45 μm, 99.999% pure, Aldrich, Milwaukee, WI) was mixed with the mullite powder specimens as an internal standard (approximately 5 wt.% Pt) to determine specimen temperature.[37,38] In order to maximize randomization of the crystallites the capillary specimens were rotated at 60 rpm.

The HTXRD patterns were subsequently analyzed by the Rietveld method[41] using the JADE software (Materials Data Inc., Livermore, CA, USA) to extract the crystallographic information as a function of temperature. The starting structural parameters and details of the prototype mullite structure were derived from Balzar and Ledbetter,[42] included as reference pattern # 74008 in the Inorganic Crystal Structure Database (NIST, Gaithersburgh, MD, USA; Fachinformationszentrum (FIZ), Karlsruhe, Germany), and are listed in Table 4. Since the objective of this study was to comprehend the thermal expansion behavior of doped mullite systems, only lattice parameters and profile function parameters of the prototype mullite structure were refined. Refinement of crystallographic site occupancies, and incorporation of metal-ion dopant in the mullite structure for complete structural analysis was considered beyond the scope of this work, and will be presented separately in a forthcoming publication.

2.3. Determination of thermal expansion coefficients

The temperature dependent evolution of lattice constants of the mullite and metal-ion doped mullite structures was used to determine thermal expansion coefficients along the different crystallographic axes. Often simple linear relationships are insufficient to describe thermal expansion over a wide temperature range, as is the case with mullite.[2] In such instances, a power series consisting of terms in ΔT, $(\Delta T)^2$ and higher order terms can be used to describe this thermal expansion over extended temperature ranges.[43] Therefore, the thermal expansion coeffi-

Table 4
Starting structure parameters[42] for analysis of crystallographic expansion of metal-ion doped mullite lattice by Rietveld refinement

Atom	No.	Oxidation state	Wyckoff position	x	y	z	Occupancy
Al	1	3	2a	0	0	0	1
Al	2	3	4h	0.1485 (1)	0.3407 (1)	0.5	0.525 (2)
Si	1	4	4h	0.1485 (1)	0.3407 (1)	0.5	0.342 (2)
Al	3	3	4h	0.2610 (7)	0.2073 (7)	0.5	0.100 (2)
Si	2	4	4h	0.2610 (7)	0.2073 (7)	0.5	0.033 (2)
O	1	−2	4h	0.3577 (2)	0.4235 (2)	0.5	1
O	2	−2	2d	0.5	0	0.5	0.475 (10)
O	3	−2	4h	0.4635 (20)	0.0465 (18)	0.5	0.198 (6)
O	4	−2	4g	0.1265 (2)	0.2197 (2)	0	1

Compound: $Al_2(Al_{2.5}Si_{1.5})O_{9.75}$; crystal symmetry, orthorhombic; S.G., *Pbam*(55). Unit cell: $a = 7.54336$ Å; $b = 7.69176$ Å; $c = 2.88402$ Å; $\alpha = \beta = \gamma = 90°$.

cient, α_n along 'nth' axis can be defined as:

$$\alpha_n = \frac{1}{l_n}\frac{\mathrm{d}l_n}{\mathrm{d}T} = A_{n,0} + A_{n,1}(T) + A_{n,2}(T^2) \quad (1)$$

where n denotes the crystallographic axes 'a', 'b' or 'c', l the lattice constant along the nth axis, and T is the temperature. Eq. (1) can be integrated over a temperature range as below:

$$\int_{l_{n,T_0}}^{l_{n,T}} \frac{\mathrm{d}l_n}{l_n} = \int_{T_0}^{T} (A_{n,0} + A_{n,1}(T) + A_{n,2}(T^2))\,\mathrm{d}T \quad (2)$$

which further yields:

$$\ln l_{n,T} = \ln l_{n,T_0} + A_{n,0}(T - T_0) + \frac{1}{2}A_{n,1}(T - T_0)^2 + \frac{1}{3}A_{n,2}(T - T_0)^3 \quad (3)$$

where $l_{n,T}$ and l_{n,T_0} are the measured lattice constants along the nth axis at temperatures T and T_0, respectively. The experimentally measured, temperature dependent evolution of lattice constants was fitted with Eq. (3) for the entire range of temperatures, by non-linear least squares routines, to determine the coefficients $A_{n,0}$, $A_{n,1}$, and $A_{n,2}$. T_0 for our study was taken as room temperature, i.e. 20 °C.

HTXRD patterns were acquired for each doped mullite specimen powder at approximately 100 °C steps, starting from room temperature up to 1400 °C. Considering the finite number of data points available for fitting in each dataset, and the 3rd order nature of Eq. (3), care was taken to avoid over parameterization. Therefore, each dataset was also fitted with 1st and 2nd order forms of Eq. (3), by setting the coefficients of higher order terms to zero. The best fit was the lowest order polynomial form of Eq. (3) which (a) resulted in minimization of residuals, (b) showed a random distribution of residual values, and (c) had reasonable error in the values of the coefficients.

3. Results and discussion

3.1. Effect of dopant ion on mullite structure

X-ray diffraction studies confirmed that mullite was the only crystalline phase present in all metal-ion doped mullite powder samples synthesized in this study. This indicated that a true solid solution had been formed. High-resolution XRD patterns were also acquired at room temperature using the CIP detector at the 33BMC beamline at APS. Lattice constants for each sample were determined by the Rietveld refinement using pure mullite (see Table 4) as the prototype structure. As stated earlier, atomic positions and site occupancies were not refined. The results are presented in Table 5, and the change in unit cell volume with concentration of dopant ions is shown in Fig. 2. The unit cell volume increased with increasing concentration of metal-ion dopants. Similar volume expansion behavior was observed for Ti- and Cr-doped samples, while Ga-doped mullites showed considerably larger expansions at higher concentrations.

Changes in lattice constants induced by metal-ion incorporation are also tabulated separately (Table 6) to highlight both the absolute and relative changes in lattice constants, with respect to pure mullite structure. Regardless of the type of metal-ion, lattice expansion was observed along the 'b' and 'c' cell edges, and increased with concentration of dopant ion. In the case of the 'a' cell edge, however, all doped mullite samples displayed

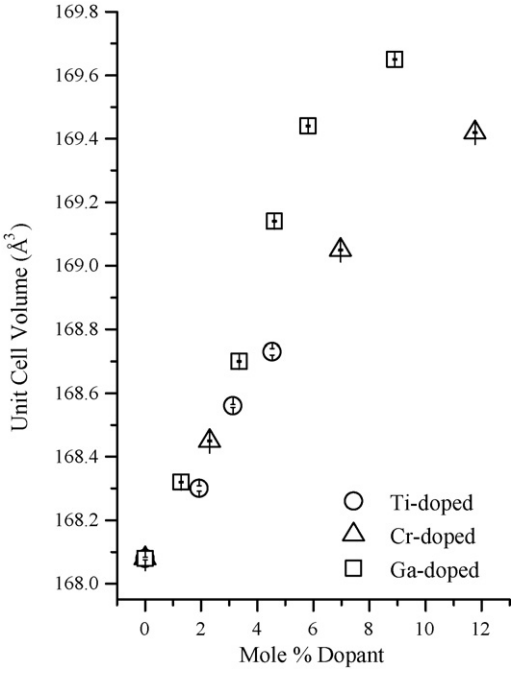

Fig. 2. Variation of unit cell volumes at room temperature with different metal-ion dopants concentrations.

Table 5
Room temperature (20 °C) lattice constants for various metal-ion doped 3:2 mullites

Phase or dopant	Sample ID	Mol% dopant cation	Lattice constants (LC) in Å		
			a	*b*	*c*
Mullite	M-0	0	7.56563 (11)	7.69505 (12)	2.88711 (4)
	Ti-1	1.93	7.56388 (23)	7.70086 (25)	2.88940 (8)
Ti	Ti-2	3.13	7.56605 (11)	7.70358 (12)	2.89204 (4)
	Ti-3	4.53	7.56627 (26)	7.70662 (29)	2.89361 (9)
	Cr-1	2.30	7.56377 (6)	7.70422 (7)	2.89063 (2)
Cr	Cr-2	6.96	7.56990 (5)	7.71032 (6)	2.89641 (2)
	Cr-3	11.76	7.57037 (5)	7.71520 (6)	2.90071 (2)
	Ga-1	1.29	7.55817 (5)	7.70804 (6)	2.88914 (2)
	Ga-2	3.35	7.56400 (5)	7.71443 (5)	2.89106 (2)
Ga	Ga-3	4.62	7.57332 (5)	7.71960 (5)	2.89312 (2)
	Ga-4	5.82	7.57628 (5)	7.72605 (5)	2.89463 (2)
	Ga-5	8.90	7.58440 (4)	7.72533 (5)	2.89546 (2)

contraction at lower dopant-ion concentrations (samples Ti-1, Cr-1, Ga-1 and Ga-2). Comparable expansion was observed along *c*-axis for all dopant ions. However, Ga-doped samples showed substantially higher expansion along *a*- and *b*-axes. With respect to pure mullite phase, the largest absolute change observed in lattice constants was along the '*b*' cell edge for all the metal-ion doped samples. The overall trend observed in absolute change in lattice constants (w.r.t. pure mullite) was similar for Ti- and Cr-doped samples (i.e. $\Delta b > \Delta c > \Delta a$). A similar trend was observed in Ga-1 and Ga-2 samples, however, for samples with higher concentrations of Ga, Δa was larger than Δc. The unit cell constants for the *a*- and *b*-axes have comparable values, while the '*c*' cell edge is less than half the size of the '*a*' or '*b*' cell edges. Therefore, relative changes in unit cell parameters are useful in understanding the impact of metal ion dopant on the mullite structure. The relative effect of Ti- and Cr-ion incorporation on the mullite structure was similar, with the observed trend being $\Delta c > \Delta b > \Delta a$. However, Ga-doping resulted in a larger (relative) change along the *b*-axis than the *c*-axis, with the trend being $\Delta b > \Delta c > \Delta a$.

Literature on the incorporation of metal-ion dopants in the mullite structure was recently summarized by Schneider and Komarneni.[2] According to past reports, up to 12 wt.% Cr_2O_3 could be incorporated into mullite.[20,23,29] In this study, up to 15.9 wt.% Cr_2O_3 was successfully incorporated in mullite. We believe that this was achievable primarily due to the more efficient mixing at molecular levels afforded by the co-precipitation method (PVA steric entrapment method) used for sample synthesis in this study. Prior studies have used reaction-sintering methods to prepare Cr-doped mullite samples, which are prone to incomplete mixing, since it has to be achieved in the solid state during prolonged annealing.

It has been stated that the relatively large cation sizes and high octahedral, but lower tetragonal, crystal field splitting parameters of most transition metal ions may explain their preference for octahedral coordination.[28] All the metal-ions evaluated in

Table 6
Change in room temperature (20 °C) lattice constants observed for metal-ion doped 3:2 mullites

Sample ID	Mol% dopant cation	Observed trend in absolute change[a] in LC w.r.t. mullite	Relative change in LC w.r.t. mullite[b]			
			Δa(%)	Δb(%)	Δc(%)	Trend
Ti-1	1.93	$\Delta b > \Delta c > \Delta a$[c]	−0.023	0.076	0.079	$\Delta c > \Delta b > \Delta a$[c]
Ti-2	3.13	$\Delta b > \Delta c > \Delta a$	0.006	0.111	0.171	$\Delta c > \Delta b > \Delta a$
Ti-3	4.53	$\Delta b > \Delta c > \Delta a$	0.008	0.150	0.225	$\Delta c > \Delta b > \Delta a$
Cr-1	2.30	$\Delta b > \Delta c > \Delta a$[c]	−0.025	0.119	0.122	$\Delta c > \Delta b > \Delta a$[c]
Cr-2	6.96	$\Delta b > \Delta c > \Delta a$	0.056	0.198	0.322	$\Delta c > \Delta b > \Delta a$
Cr-3	11.76	$\Delta b > \Delta c > \Delta a$	0.063	0.262	0.471	$\Delta c > \Delta b > \Delta a$
Ga-1	1.29	$\Delta b > \Delta c > \Delta a$[c]	−0.099	0.169	0.070	$\Delta b > \Delta c > \Delta a$[c]
Ga-2	3.35	$\Delta b > \Delta c > \Delta a$[c]	−0.022	0.252	0.137	$\Delta b > \Delta c > \Delta a$[c]
Ga-3	4.62	$\Delta b > \Delta a > \Delta c$	0.102	0.319	0.208	$\Delta b > \Delta c > \Delta a$
Ga-4	5.82	$\Delta b > \Delta a > \Delta c$	0.141	0.403	0.260	$\Delta b > \Delta c > \Delta a$
Ga-5	8.90	$\Delta b > \Delta a > \Delta c$	0.248	0.393	0.289	$\Delta b > \Delta c > \Delta a$

[a] Absolute changes in LC are: $\Delta a = (a - a_0)$; $\Delta b = (b - b_0)$; $\Delta c = (c - c_0)$; where a_0, b_0, and c_0 are lattice constants of pure mullite phase (Sample M-0 from Table 5).

[b] Relative changes in LC are: $\Delta a = (a - a_0)/a_0$; $\Delta b = (b - b_0)/b_0$; $\Delta c = (c - c_0)/c_0$; where a_0, b_0, and c_0 are lattice constants of pure mullite phase (Sample M-0 from Table 5).

[c] These values were negative.

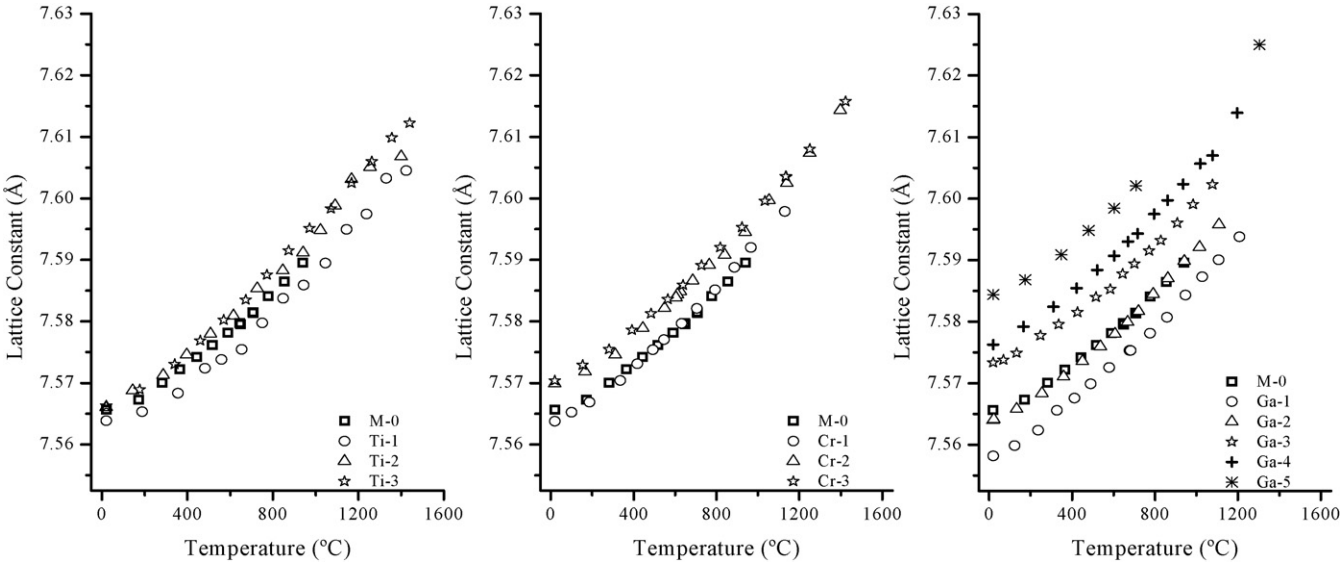

Fig. 3. Evolution of lattice constant with temperature along the *a*-axis for different types of metal-ion doped 3:2 mullite samples for a range of concentrations.

this study, i.e. Ti^{4+}, Cr^{3+} and Ga^{3+} have a stable electron configuration (see Table 2) with a spherically symmetrical charge distribution. As a result, the structural position for their inclusion in mullite should be essentially controlled by the size of the cations. Replacement of Al^{3+} from the AlO_6 octahedra was suggested as a possible mechanism for metal-ion incorporation. Substitution of Al^{3+} with a larger cation in oxygen octahedra should produce a larger expansion along the *b*-axis than along the *a*-axis, which is also considered to be 'normal expansion' behavior. The incorporation-induced structural expansion in mullite structure observed for all the metal-ion doped mullite samples in this study showed a larger change in '*b*' cell edge than in the '*a*' cell edge, i.e. $\Delta b > \Delta a$. This observation is consistent with the substitution of Al^{3+} in the AlO_6 octahedra by Ti^{4+}, Cr^{3+}, and Ga^{3+} ions as a possible mechanism for their incorporation in mullite. Further evaluation of other possible mechanisms for metal-ion incorporation in mullite, such as occupation of regular and interstitial sites by Cr^{3+} at higher concentrations, require in-depth crystallochemical analysis and was considered beyond the scope of the present study.

The contraction observed along the *a*-axis for low dopant ion concentrations is consistent with earlier studies where the metal-ion doped mullite samples were synthesized using the sol–gel method for sample preparation.[17,27] Schneider and Vasudevan[27] have reported a similar contraction in *a*-axis in Mn^{3+} ion doped mullites, and have suggested the distortion of octahedra due to the Jahn–Teller effect, as a possible explanation. Polyhedral distortion at low metal-ion concentrations could explain the observed contraction along the *a*-axis. Since all the metal ions considered in this study have stable electron configurations, distortion of polyhedra as a result of crystal field stabilization is not possible, as was the case in Mn^{3+} ions. However, other

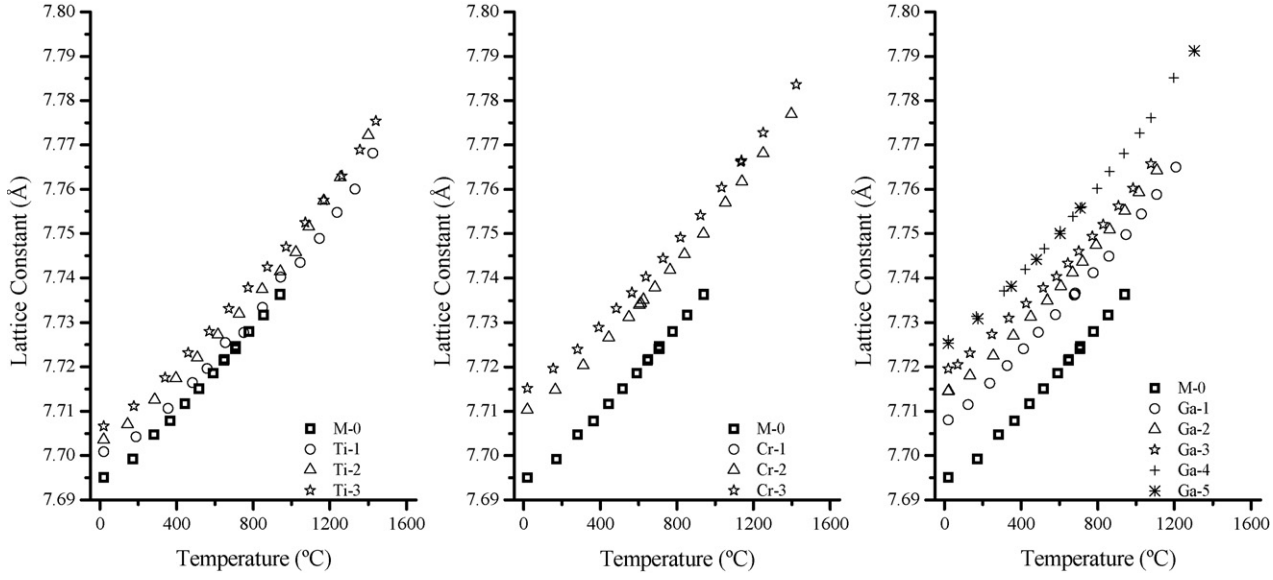

Fig. 4. Evolution of lattice constant with temperature along the *b*-axis for different types of metal-ion doped 3:2 mullite samples for a range of concentrations.

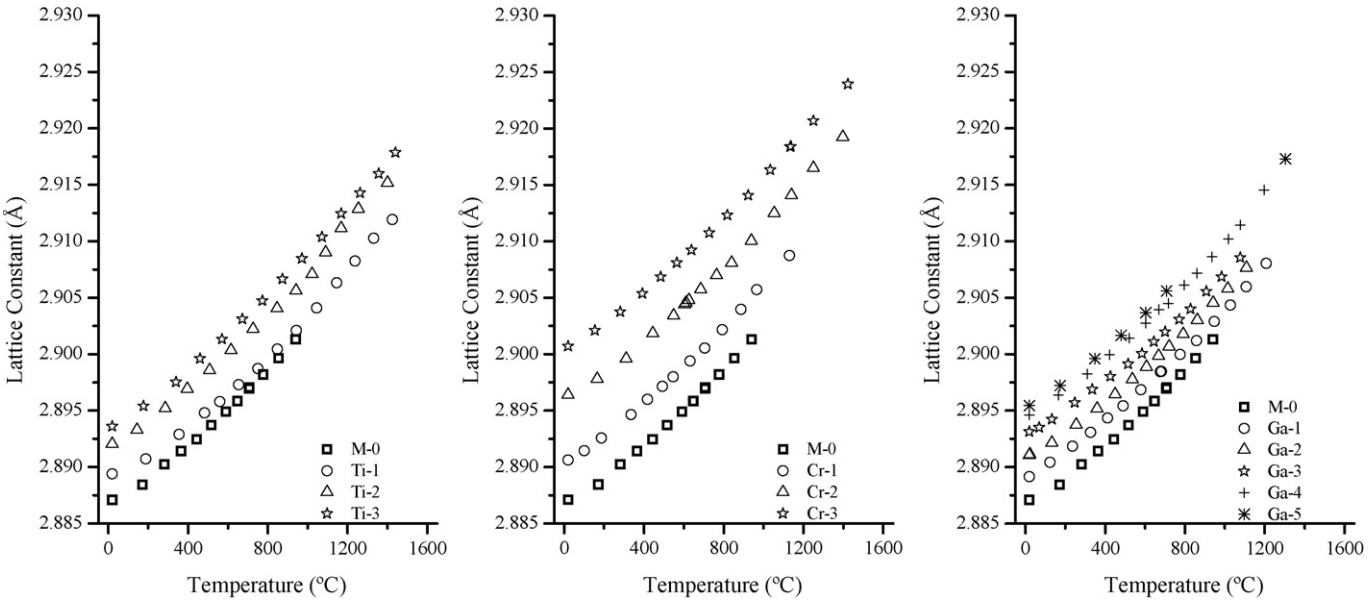

Fig. 5. Evolution of lattice constant with temperature along the *c*-axis for different types of metal-ion doped 3:2 mullite samples for a range of concentrations.

crystal chemical phenomena, such ionization, cation repulsion across shared anion bridges, etc., can also induce distortion in polyhedra.

3.2. Thermal expansion of metal-ion doped mullites

HTXRD patterns were acquired for all the 12 samples, although, over slightly different temperature ranges, and analyzed using the Rietveld method.[41] The evolution of lattice constants with temperature, along each crystallographic axis, and the variation of unit cell volume with temperature is plotted for all the samples in Figs. 3–6. For clarity and better comparison, the lattice expansion for each of the three types of metal-ion doped mullites is presented separately using the same scale. The lattice expansion of pure mullite phase, prepared by the sol–gel method (sample M-0), is also included on each graph for comparison.

In the temperature range extending from room temperature (RT) to 1000 °C, comparison of the relative elongation or axial expansion (i.e. $\Delta a/a_{RT}$ or $\Delta b/b_{RT}$ or $\Delta c/c_{RT}$ expressed as %), is a good indicator of the effect of metal-ion on mullite lattice expansion. The largest elongation was observed along the *b*-axis (i.e. $\Delta b/b_{RT}$) for all the samples and was fairly similar to that observed in pure mullite phase (~0.5%). The mullite lattice expanded the least along the *a*-axis for all the samples ($0.28\% \leq \Delta a/a_{RT} \leq 0.41\%$), with the measured value for mullite being 0.32%. These observations are consistent with earlier reports by Schneider and Eberhard[14] and Brunauer et

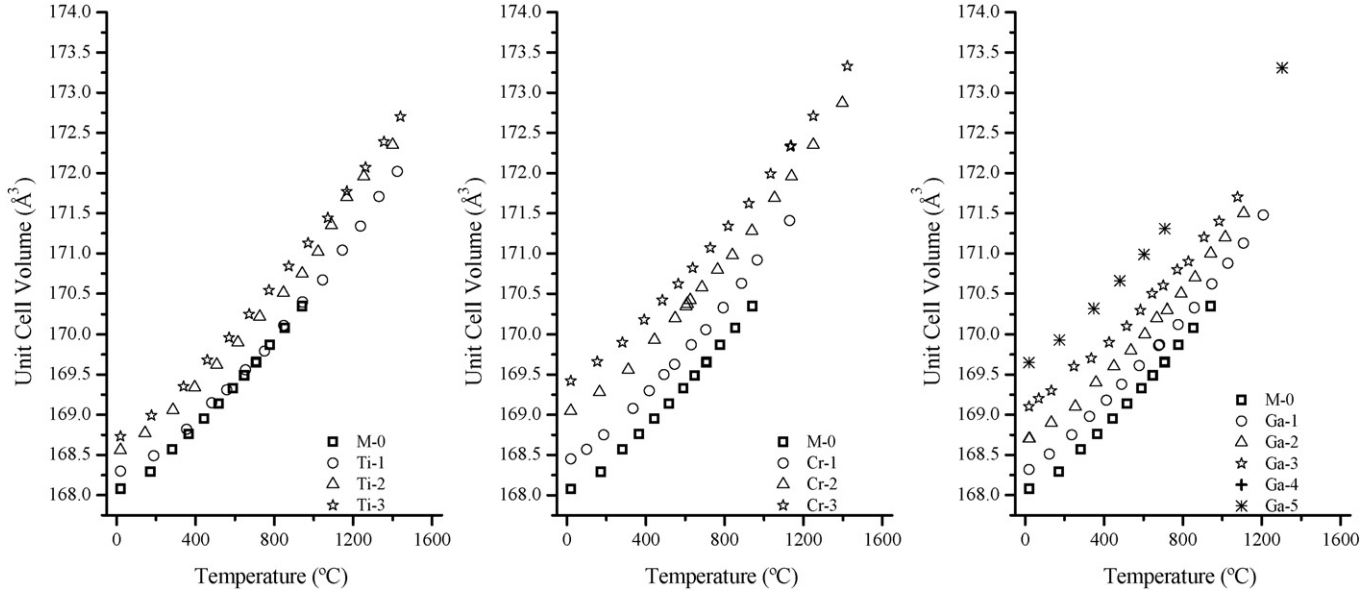

Fig. 6. Evolution of unit cell volume with temperature for different types of metal-ion doped 3:2 mullite samples for a range of concentrations.

Table 7
Thermal expansion coefficients measured for types of metal-ion doped 3:2 mullite samples for a range of concentrations

Phase or dopant	Sample ID	Mol% dopant cation	Thermal expansion coefficients [$\alpha_n = A_{n,0} + A_{n,1}(T-20)$; $\beta = B_0 + B_1(T-20)$; where n is for a, b, or c axis]										Temperature range (°C)
			α_a		α_b		α_c		α_{mean} [a]		β		
			$A_{a,0} \times 10^{-6}$	$A_{a,1} \times 10^{-9}$	$A_{b,0} \times 10^{-6}$	$A_{b,1} \times 10^{-9}$	$A_{c,0} \times 10^{-6}$	$A_{c,1} \times 10^{-9}$	$A_0 \times 10^{-6}$	$A_1 \times 10^{-9}$	$B_0 \times 10^{-6}$	$B_1 \times 10^{-9}$	
Mullite	M-0	0.00	1.88 (3)	3.42 (8)	4.40 (3)	3.23 (8)	3.67 (3)	3.68 (7)	3.32 (2)	3.44 (5)	10.20(5)	9.7(1)	20–1000
	Ti-1	1.93	1.63 (5)	3.28 (7)	3.45 (5)	3.83 (8)	3.19 (4)	3.40 (6)	2.76(3)	3.51(4)	8.29(8)	10.5(1)	20–1400
Ti	Ti-2	3.13	2.98 (2)	1.62 (3)	3.79 (2)	3.78 (3)	3.93 (2)	2.81 (3)	3.57(1)	2.74(2)	10.77(3)	8.14(5)	20–1400
	Ti-3	4.53	3.00 (4)	1.85 (6)	4.13 (4)	2.92 (6)	4.25 (3)	2.31 (5)	3.79(2)	2.36(3)	11.34(6)	7.12(9)	20–1400
	Cr-1	2.30	2.56 (1)	2.81 (3)	4.36 (1)	3.15 (3)	4.062 (9)	2.91 (2)	3.661(6)	2.96(1)	10.88(2)	9.04(4)	20–1100
Cr	Cr-2	6.96	2.313 (9)	2.80 (2)	4.45 (1)	2.62 (2)	3.900 (8)	2.71 (2)	3.556(5)	2.71(1)	10.69(2)	8.12(3)	20–1400
	Cr-3	11.76	2.558 (9)	2.44 (2)	4.344 (9)	2.79 (2)	3.965 (7)	2.56 (1)	3.622(5)	2.596(9)	10.85(1)	7.84(3)	20–1400
	Ga-1	1.29	2.745 (9)	2.07 (2)	4.81 (1)	2.28 (2)	4.113 (8)	2.25 (2)	3.889(5)	2.20(1)	11.59(2)	6.71(3)	20–1200
	Ga-2	3.35	2.31 (1)	2.93 (3)	4.40 (1)	2.84 (3)	3.77 (1)	2.74 (2)	3.491(6)	2.84(2)	10.44(2)	8.58(5)	20–1100
Ga	Ga-3	4.62	2.12 (1)	2.85 (3)	4.00 (1)	3.02 (3)	3.50 (1)	2.87 (2)	3.207(6)	2.91(2)	9.62(2)	8.74(5)	20–1100
	Ga-4	5.82	2.42 (1)	2.97 (2)	4.39 (1)	3.42 (2)	3.803 (8)	3.30 (2)	3.536(5)	3.23(1)	10.55(2)	9.75(4)	20–1200
	Ga-5	8.90	2.32 (1)	2.87 (2)	4.58 (1)	3.19 (2)	4.03 (1)	2.84 (2)	3.642(6)	2.97(1)	10.86(2)	8.98(3)	20–1300

[a] For α_{mean}, $A_0 = (A_{a,0} + A_{b,0} + A_{c,0})/3$; $A_1 = (A_{a,1} + A_{b,1} + A_{c,1})/3$.

al.[13] Increase in Ti^{4+} ion concentration resulted in an increase in axial expansion measured along all the axes and consequently the unit cell volume. In contrast, the increase in concentration of Cr^{3+} ion resulted in a decrease in axial expansion along all the axes. The concentration of Ga^{3+} ion did not have any significant effect on axial expansion in this temperature range, and the values were comparable to those of the pure mullite phase. In order to evaluate the effect of different metal-ion dopants on thermal expansion of the mullite lattice, it is reasonable to compare the expansion of Ti-3, Cr-2, and Ga-3 samples, as they have approximately 4.5 mol% composition (except for Cr-2 sample which had 6.96 mol% Cr^{3+} ion). Both Cr-2 and Ga-3 samples showed very similar axial expansion behavior, similar to that of pure mullite (sample M-0). However, in the case of the Ti-3 sample, larger axial expansion was observed along all the axes, particularly along the *c*-axis (0.66%).

In the absence of any consensus on phase transformations in mullite,[2] as well as the reported non-linearity in thermal expansion of mullite at lower (<300 °C) and higher temperatures (>1000 °C),[14] a continuous curve was considered appropriate to model the thermal expansion behavior. The lattice expansion was fitted with a continuous curve using Eq. (3). Using the criteria stated earlier in this article, the 2nd order form of Eq. (3) was found most suitable to model thermal expansion of mullite samples from room temperature up to 1400 °C. Therefore, it is proposed that the thermal expansion of mullite and metal-ion doped mullites has a linear dependence on temperature (i.e. $\alpha(T) = A_0 + A_1 \Delta T$). Results are summarized in Table 7 as values for the $A_{n,0}$ and $A_{n,1}$ coefficients for α_n, where '*n*' denotes '*a*', '*b*' or '*c*' crystallographic axis for mullite. Also included are the values for the coefficients A_0 and A_1 for α_{mean} and the B_0 and B_1 coefficients, which define the volume expansion coefficient β.

A distinct trend was apparent in the values of the coefficients with concentration of the dopant ion, as well as for different metal-ion types (Table 7). With an increase in concentration of the dopant ion, the A_0 values were found to increase along all the crystallographic axes in the case of Ti-doped mullites, while the values remained fairly constant and similar for the Cr- and Ga-doped samples. The values of the A_1 coefficients, which determine the change in thermal expansion coefficients with temperature, showed a different trend altogether. In the case of the Ti- and Cr-doped samples, the A_1 coefficient values decreased with increase in dopant ion concentration along all the three axes. In contrast, the A_1 values showed a small increase with Ga^{3+} ion concentration. In order to compare the effect of the type of dopant ion on B_0 and B_1 coefficients, the values from Ti-3, and Ga-3 samples were compared with Cr-2* sample. The *B* coefficients for Cr-2* sample were calculated for 4.6 mol% of Cr^{3+} ion concentration by interpolation. The comparison is presented in Fig. 7. With an increase in the ionic radii of the dopant metal-ion, the B_0 coefficient decreased (≈15%), while the B_1 coefficient increased (≈23%).

The effect of type of metal-ion dopant on the mean thermal expansion (α_{mean}) behavior is presented in Fig. 8 for samples with approximately 4.6 mol% metal-ion dopant concentration (i.e. samples Ti-3, Cr-2* and Ga-3). In the temperature range

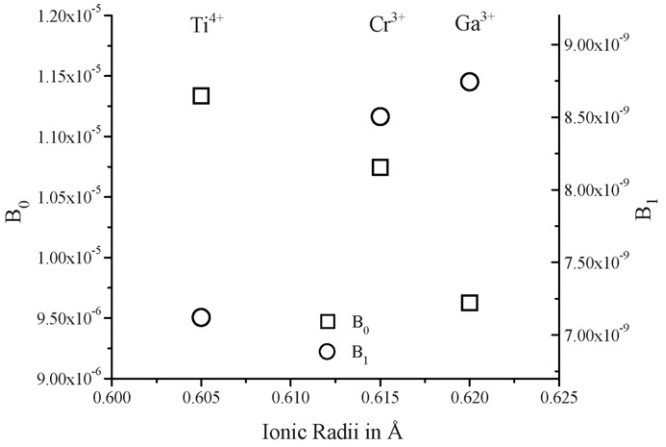

Fig. 7. Variation of B_0 and B_1 coefficients with ionic radii of the metal-ions doped in the mullite structure. These coefficients define the linear temperature dependent volume expansion (β) behavior of mullite according to the equation $\beta = B_0 + B_1(T - 20)$, where *T* is the temperature in °C.

from room temperature to 1000 °C, the α_{mean} values increased with temperature and were within 3.0–6.7 for all the samples. The α_{mean} values for metal-ion doped samples were smaller at higher temperatures in comparison with the pure mullite phase. The α_{mean} values for the Cr-2* and the Ga-3 samples showed a similar temperature dependence, which was different from the Ti-doped or the pure mullite samples. The resemblance in the evolution of α_{mean} values with temperature for the Cr-2* and the Ga-3 samples is most likely due to the similarities in the way in which Cr^{3+} and Ga^{3+} are incorporated into and influence the mullite structure.

Structure-controlled expansion anisotropy (A-factor) is an important parameter, which can provide further insight into the understanding of the thermal expansion behavior of ceramics.[14]

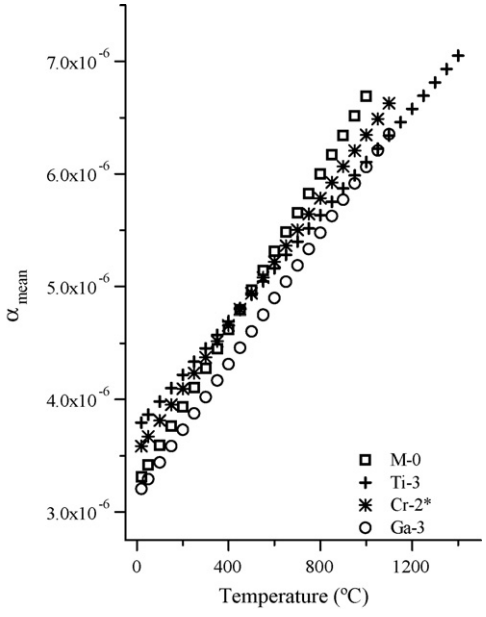

Fig. 8. The effect of type of metal-ion dopant on the mean thermal expansion (α_{mean}) behavior for samples with approximately 4.5 mol% metal-ion dopant concentrations.

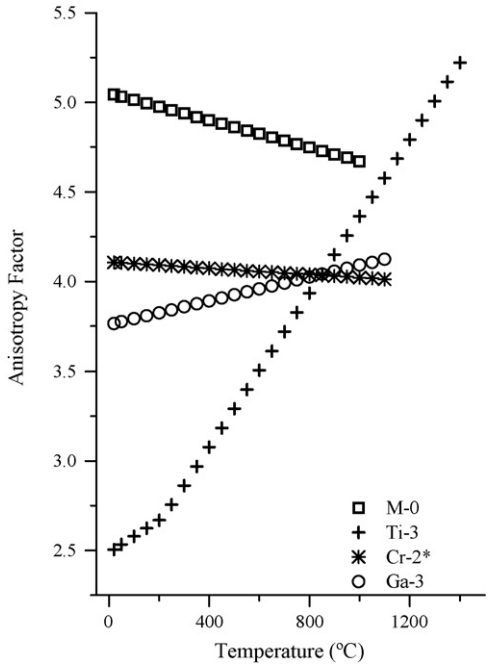

Fig. 9. The effect of type of metal-ion dopant on the anisotropy factor (A-factor). The plots are for samples with ~4.5 mol% concentration of the dopant ion.

The effect of type of metal-ion dopant on the A-factor is presented in Fig. 9. In the temperature range from RT to 1000 °C, the A-factor of mullite was higher than the Cr- and Ga-doped samples. The A-factor for mullite, Cr- and Ga-doped mullites did not show much variation in this temperature range. The A-factor for the Ti-doped mullite samples, however, extended from ~2.5 at temperatures <200 °C to ~4.5 at 1000 °C, and increased further at higher temperatures. The increase in anisotropy factor in the case of Ti-doped sample is perhaps attributable to the 4+ oxidation state of the Ti ion, and its incorporation into the mullite structure at the Al^{3+} position in the AlO_6 octahedra. Moreover, substitution of Si^{4+} by Al^{3+} in the SiO_4 tetrahedra, in order to compensate for the charge imbalance caused by Ti^{4+} incorporation,[28] may also be responsible for the enhanced anisotropy exhibited by the Ti-doped sample.

Thermal expansion measurements can also be considered as an indirect probe of the bond strength and bonding environment in a material system. The variability in bond strength along different directions, for example in the AlO_6 octahedra in mullite, could explain the differences observed in the thermal expansion behavior measured along different crystallographic axis, and hence the anisotropy. The replacement of Al^{3+} in the oxygen octahedra with different metal-ions (i.e. Ti^{4+}, Cr^{3+}, or Ga^{3+}) should modify the bonding environment locally and result in different bond strengths and consequently different thermal expansion. The A_0 and B_0 coefficients define the thermal expansion at the chosen reference temperature (i.e. 20 °C in this study). Thus these values are representative of the effect of bonding environment at this temperature. However, change in a thermal expansion coefficient with temperature should require a temperature dependent change in local bonding environment. For thermal expansion that is linearly dependent on temperature, as observed in this study, the A_1 and B_1 coefficients are the rate of change of thermal expansion with temperature, and therefore should represent the effect of change in the local bonding environment on thermal expansion with temperature. We believe that the A_1 and B_1 parameters can provide valuable insight into the mechanism of thermal expansion in this material system. However, this would also require detailed crystallochemical analysis of mullite and doped mullite structures with temperature, and is a subject of further study.

4. Conclusions

In this work, the effect of transition metal-ion doping on thermal expansion of 3:2 mullite was studied by HTXRD using synchrotron radiation up to 1400 °C in air. Three metal-ion dopants, which had very similar ionic radii, but different oxidation states and electronic configurations, were evaluated in this study, and included Ti^{4+}, Cr^{3+}, and Ga^{3+}. Using the co-precipitation methods single phase mullite and metal-ion doped mullite samples were synthesized, and up to 15.9 wt.% Cr_2O_3 was successfully incorporated in mullite.

The induced structural expansion due to transition metal-ion incorporation in mullite structure was larger along the '*b*' cell edge than the '*a*' cell edge, i.e. $\Delta b > \Delta a$ in all the samples. This observation is consistent with the substitution of Al^{3+} in the AlO_6 octahedra by Ti^{4+}, Cr^{3+}, and Ga^{3+} ions and conforms to the proposed mechanism for their incorporation in mullite.[2] The effect of Ti- and Cr-ion incorporation on the mullite structure was similar, with the observed trend in relative expansion along different crystallographic axes being $\Delta c > \Delta b > \Delta a$. However, Ga-doping resulted in a larger (relative) change along the *b*-axis than the *c*-axis, with the trend being $\Delta b > \Delta c > \Delta a$.

Thermal expansion behavior of 3:2 mullite was studied as a function of both the type and the concentration of transition metal-ion dopant using HTXRD. In the temperature range from 20 °C to 1000 °C, the largest elongation was observed along the *b*-axis and was fairly independent of the type and concentration of the metal-ion dopant. The mullite lattice expanded the least along the *a*-axis. With an increase in Ti^{4+} ion concentration, an increase in axial expansion was observed along all the axes, whereas the increase in concentration of Cr^{3+} ion resulted in a decrease in axial expansion along all the axes. The concentration of Ga^{3+} ion did not have any significant effect on axial expansion in this temperature range, and the values were comparable to those of the pure mullite phase.

Based on rigorous statistical analysis of thermal evolution of lattice parameters, it was concluded that the thermal expansion of mullite and metal-ion doped mullites has a linear dependence on temperature (i.e. $\alpha(T) = A_0 + A_1 \Delta T$). In the temperature range from room temperature to 1000 °C, the α_{mean} values increased with temperature and were within 3.0–6.7 for all the samples. The α_{mean} values for metal-ion doped samples were smaller at higher temperatures in comparison with those of the pure mullite phase. The evolution of α_{mean} values with temperature for the Cr- and the Ga-doped samples with approximately 4.5 mol% metal-ion dopant concentration suggests similarities in the way

in which Cr^{3+} and Ga^{3+} are incorporated into, and influence the mullite structure.

We believe that this study is unique in its comprehensive approach and in defining a methodology for reporting and understanding the thermal expansion properties of mullite systems. Most of the findings reported in this investigation are consistent with existing literature, and lay the foundation for future research in the advancement of knowledge on the thermal behavior of mullite systems based on crystal chemical analysis.

Acknowledgments

Initial discussions with Dr. Hartmut Schneider are gratefully acknowledged. This work was supported by the Air Force Office of Scientific Research, USAF. Yoon was supported under AFOSR Grant no. F49620-03-1-0082; Bhorkar was supported under AFOSR MEANS Grant no. F 49620-01-0500; Chiritescu was supported by AFOSR STTR Grant no. F49620-02-C-0016 (Subcontract AF-STTR 01-NA-240). Sarin was supported by funds from the National Science Foundation (DMR 02-11139). Use of the facilities in the Center for Microanalysis of Materials, University of Illinois, which is partially supported by the U.S. Department of Energy under grant DEFG02-91-ER45439 and the APS, Argonne National Laboratory is supported by the US DOE, BES Materials Sciences, under Contract no: W-31-109-ENG-38 are gratefully acknowledged. The authors would also like to sincerely thank the authors of the book "Mullite"[2] as it provided an excellent resource on the current understanding of this material system.

References

[1]. Aksay, I. A., Dabbs, D. M. and Sarikaya, M., Mullite for structural, electronic, and optical applications. *Journal of the American Ceramic Society*, 1991, **74**(10), 2343–2358.

[2]. Schneider, H. and Komarneni, S., ed., *Mullite*. Wiley-VCH, Weinheim, Germany, 2005, p. 487.

[3]. Cameron, W. E., Mullite: a substituted alumina. *American Mineralogist*, 1977, **62**, 747–755.

[4]. Fischer, R. X., Schneider, H. and Voll, D., Formation of aluminum rich 9:1 mullite and its transformation to low alumina mullite upon heating. *Journal of the European Ceramic Society*, 1996, **16**(2), 109–113.

[5]. Angel, R. J. and Prewitt, C. T., Crystal-structure of mullite—a reexamination of the average structure. *American Mineralogist*, 1986, **71**(11–12), 1476–1482.

[6]. Burnham, C. W., *Crystal Structure of Mullite*, *Vol. 62*. Carnegie Institute of Washington, 1963, Yearbook, pp. 158–165.

[7]. Burnham, C. W., *Crystal Structure of Mullite*, *Vol. 63*. Carnegie Institute of Washington, 1964, Yearbook, pp. 223–228.

[8]. Durovic, S. and Fejdi, P., Synthesis and crystal structure of germanium mullite and crystallochemical parameters of D-mullites. *Silikaty*, 1976, **20**, 97–112.

[9]. Saalfeld, H. and Guse, W., Structure refinement of 3-2-mullite ($3Al_2O_3{\cdot}2SiO_2$). *Neues Jahrbuch Fur Mineralogie-Monatshefte*, 1981(4), 145–150.

[10]. Aksay, I. A. and Pask, J. A., Stable and metastable equilibria in the system SiO_2–Al_2O_3. *Journal of the American Ceramic Society*, 1975, **58**(11–12), 507–512.

[11]. Kriven, W. M. and Pask, J. A., Solid-solution range and microstructures of melt-grown mullite. *Journal of the American Ceramic Society*, 1983, **66**(9), 649–654.

[12]. Sanyal, D., Banerjee, D., Bhattacharya, R., Patra, S. K., Chaudhuri, S. P., Ganguly, B. N. and De, U., Study of transition metal ion doped mullite by positron annihilation techniques. *Journal of Materials Science*, 1996, **31**(13), 3447–3451.

[13]. Brunauer, G., Frey, F., Boysen, H. and Schneider, H., High temperature thermal expansion of mullite: an in situ neutron diffraction study up to 1600 degrees C. *Journal of the European Ceramic Society*, 2001, **21**(14), 2563–2567.

[14]. Schneider, H. and Eberhard, E., Thermal-expansion of mullite. *Journal of the American Ceramic Society*, 1990, **73**(7), 2073–2076.

[15]. Baudin, C., Osendi, M. I. and Moya, J. S., Solid-solution of TiO_2 in mullite. *Journal of Materials Science Letters*, 1983, **2**(5), 185–187.

[16]. Caballero, A. and Ocana, M., Synthesis and structural characterization by X-ray absorption spectroscopy of tin-doped mullite solid solutions. *Journal of the American Ceramic Society*, 2002, **85**(8), 1910–1914.

[17]. Chaudhuri, S. P. and Patra, S. K., Preparation and characterisation of transition metal ion doped mullite. *British Ceramic Transactions*, 1997, **96**(3), 105–111.

[18]. Das, P. and Choudhury, R., Studies on the variation of cell dimensions of mullite with iron-oxide and titania additions. *X-Ray Spectrometry*, 1988, **17**(5), 187–188.

[19]. Green, C. R. and White, J., Solid solubility of TiO_2 in mullite in the system Al_2O_3–TiO_2–SiO_2. *Transactions of the British Ceramic Society*, 1974, **73**, 73–75.

[20]. Murthy, M. K. and Hummel, F. A., X-ray study of the solid solution of TiO_2, Fe_2O_3, and Cr_2O_3 in mullite ($3Al_2O_3{\cdot}2SiO_2$). *Journal of the American Ceramic Society*, 1960, **43**, 267–273.

[21]. Ocana, M., Caballero, A., Gonzalez-Carreno, T. and Serna, C. J., Preparation by pyrolysis of aerosols and structural characterization of Fe-doped mullite powders. *Materials Research Bulletin*, 2000, **35**(5), 775–788.

[22]. Rager, H., Schneider, H. and Bakhshandeh, A., Ti^{3+} centers in mullite. *European Journal of Mineralogy*, 1993, **5**(3), 511–514.

[23]. Rager, H., Schneider, H. and Graetsch, H., Chromium incorporation in mullite. *American Mineralogist*, 1990, **75**(3–4), 392–397.

[24]. Schneider, H., Solubility of TiO_2, Fe_2O_3 and MgO in mullite. *Ceramics International*, 1987, **13**(2), 77–82.

[25]. Schneider, H. and Rager, H., Occurrence of Ti-3+ and Fe-2+ in mullite. *Journal of the American Ceramic Society*, 1984, **67**(11), C248–C250.

[26]. Schneider, H. and Rager, H., Iron incorporation in mullite. *Ceramics International*, 1986, **12**(3), 117–125.

[27]. Schneider, H. and Vasudevan, R., Structural deformation of manganese substituted mullites—X-ray-line broadening and lattice-parameter studies. *Neues Jahrbuch Fur Mineralogie-Monatshefte*, 1989(4), 165–178.

[28]. Schneider, H., Transition metal distribution in mullite. In *Mullite and Mullite Matrix Composites*, ed. S. Somiya, R. F. Davis and J. A. Pask. The American Ceramic Society, Westerville, OH, 1990, pp. 135–157.

[29]. Gelsdorf, G., Müller-Hesse, H. and Schwiete, H. E., Einlagerungsversuche an synthetischem Mullit und ubstitutionsversuche mit Galliumoxyd und Germaniumoxyd. *Teil II. Arch. Eisenhüttenwesen*, 1958, **29**, 513–519.

[30]. Schreuer, J., Hildmann, B. and Schneider, H., Elastic properties of mullite single crystals up to 1400 degrees C. *Journal of the American Ceramic Society*, 2006, **89**(5), 1624–1631.

[31]. Gulgun, M. A. and Kriven, W. M., A simple solution polymerization route for oxide powder synthesis. In *Ceramic Transactions*, *Vol. 62*, ed. J. J. Kingsley, C. H. Schilling and J. H. Adair. The American Ceramic Society, 1995, pp. 57–66.

[32]. Gulgun, M. A., Kriven, W. M. and Nguyen, M. H., Processes for preparing mixed oxide powders. U.P. Office, Editor, 2002: USA.

[33]. Gulgun, M. A., Nguyen, M. H. and Kriven, W. M., Polymerized organic–inorganic synthesis of mixed oxides. *Journal of the American Ceramic Society*, 1999, **82**(3), 556–560.

[34]. Kriven, W. M., Lee, S. J., Gulgun, M. A., Nguyen, M. H. and Kim, D.-K., Synthesis of oxide powders via polymeric steric entrapment. In *Ceramic Transactions*, *Vol. 108*, ed. J. P. Singh, N. P. Bansal and K. Niihara. The American Ceramic Society, 1999, pp. 99–110.

[35]. Kriven, W. M., Rosczyk, B. R., Bertoni, M. I. and Mason, T. O., Synthesis of mixed conducting oxides by an organic steric entrapment method. In *Ceramic Engineering and Science Proceedings: 27th International Cocoa*

Beach Conference on Advanced Ceramics and Composites: A, Vol. 24, ed. W. M. Kriven and H. T. Lin, 2003, pp. 287–292.

[36]. Lee, S.-J. and Kriven, W. M., Preparation of ceramic powders by a solution-polymerization route employing PVA solution. *Ceramic Engineering and Science Proceedings*, 1998, **19**(4), 469–476.

[37]. Sarin, P. Y., Jurkschat, W. K., Zschack, P. and Kriven, W. M., Quadrupole lamp furnace for high temperature (up to 2050 K) synchrotron powder X-ray diffraction studies in air. *Review of Scientific Instruments*, 2006, **77**(9), 093906.

[38]. Siah, L. F., Kriven, W. M. and Schneider, J., In situ, high-temperature, synchrotron, powder diffraction studies of oxide systems in air, using a thermal-image furnace. *Measurement Science and Technology*, 2005, **16**, 1–8.

[39]. Sarin, P., Haggerty, R. P., Yoon, W., Knapp, M., Berghauser, A., Zschack, P. and Kriven, W.M., A curved image plate detector system for high resolution synchrotron X-ray diffraction. *Journal of Synchrotron Radiation*, in preparation.

[40]. Sarin, P., Haggerty, R. P., Yoon, W., Zschack, P., Knapp, M. and Kriven, W. M., Rapid in situ ultra-high temperature investigations of ceramics using synchrotron X-ray diffraction. *Ceramic Engineering Science Proceedings*. The American Ceramic Society, Westerville, OH, 2006, pp. 313–324.

[41]. Rietveld, H. M., A profile refinement method for nuclear and magnetic structures. *Journal of Applied Crystallography*, 1969, **2**, 65–71.

[42]. Balzar, D. and Ledbetter, H., Crystal-structure and compressibility of 3-2 mullite. *American Mineralogist*, 1993, **78**(11–12), 1192–1196.

[43]. Newnham, R. E., *Properties of Materials: Anisotropy, Symmetry, Structure*. Oxford University Press, New York, NY, 2005, p. 378.

[44]. Shannon, R. D., Revised effective ionic radii and systematic studies of interatomie distances in halides and chaleogenides. *Acta Crystallographica*, 1976, **32**, 751–767.

[45]. Vainshtein, B. K., Fridkin, V. K. and Indenbom, V. L. ed., *Structure of Crystals. Modern Crystallogrphy*, *Vol. 2*. 3rd ed. Springer-Verlag, Berlin, Germany, 2000, p. 520.